PRECONDITIONED INTENSITY-BASED PROSTATE REGISTRATION USING STATISTICAL DEFORMATION MODELS

Oliver Zettinig[1*], *Julia Rackerseder*[1], *Beatrice Lentes*[1], *Tobias Maurer*[2]
Kay Westenfelder[2], *Matthias Eiber*[3], *Benjamin Frisch*[1], *Nassir Navab*[1,4]

[1] Computer Aided Medical Procedures, Technische Universität München, Germany
[2] Urologische Klinik und Poliklinik, Technische Universität München, Germany
[3] Nuklearmedizin, Technische Universität München, Germany
[4] Computer Aided Medical Procedures, Johns Hopkins University, Baltimore, USA

ABSTRACT

Despite the common invisibility of cancerous lesions in transrectal ultrasound (TRUS), TRUS-guided random biopsy is considered the gold standard to diagnose prostate cancer. Pre-interventional magnetic resonance imaging (MRI) has been shown to improve the detection of malignancies but fast and accurate MRI/TRUS registration for multi-modal biopsy guidance remains challenging. In this work, we derive a statistical deformation model (SDM) from 50 automatically segmented patient datasets and propose a novel registration scheme based on a lesion-specific, anisotropic preconditioned similarity metric. The approach is validated on a dataset of 10 patients, showing landmark registration errors of 1.41 mm in the vicinity of suspicious areas.

Index Terms— Prostate, Registration, Statistical Deformation Model, Preconditioning

1. INTRODUCTION

The current gold standard for prostate cancer diagnosis relies on 12-core random biopsies under TRUS guidance [1]. The invisibility of many lesions in ultrasound contributes greatly to the low sensitivity of the method. Thus, multi-modal approaches including magnetic resonance imaging (MRI) and, more recently, positron emission tomography (PET) with specific tracers targeting the prostate specific membrane antigen (PSMA) are utilized to identify suspicious lesions in pre-interventional images, and to aid their targeting during the biopsy [2]. Recent studies, suggesting that accurate MRI/TRUS registration outperforms cognitive fusion by the physicians to target cancerous lesions, drive the ongoing development of image fusion-guided biopsy systems [3].

This registration has been the topic of many prior studies. Fiducial-based approaches as in [4] as well as surface-based methods such as [5, 6] require manual annotations or segmentations in at least one of two images, and yield affine or spline-interpolated elastic image alignment. Such algorithms inherently neglect inhomogeneous deformations within the prostate gland.

One option to overcome this limitation is to perform a deformable intensity-based registration between both images, see the review by Sotiras et al. [7] and references therein. Focusing on geometric constraints of the transformation model, proposed methods are either based on control points and an interpolation scheme [8] or on a dense, voxel-wise formulation of the deformation field [9]. In either case, non-linear deformation models regularly include a high number of parameters, with known challenges in overcoming local minima, on physically reasonable regularization.

The availability of sufficiently large annotated datasets of various anatomies has often been exploited to generate statistical models of shape, texture and deformation as priors for deformable registration, effectively reducing the dimensionality of the optimization problem while at the same time enforcing physically meaningful deformations [7].

A learning technique is used for dimensionality reduction, for instance in the case of principal component analysis (PCA) allowing to optimize an unseen dataset's representation in PCA space. While the work of Onofrey et al. [10] allows for a MRI/TRUS registration using a population-based statistical deformation model, the algorithm is point-based and does not consider image intensities.

A popular choice to generate patient-specific statistical models of prostate motion is biomechanical simulation [11, 12] based on prior segmentations in MRI. Such approaches regularly require a large quantity of finite element simulations for a wide range of TRUS probe positions. Even if population data is used for the simulations, MRI segmentations are required for personalization of unseen datasets [13]. However, due to time constraints and the large inter-observer variation [3],
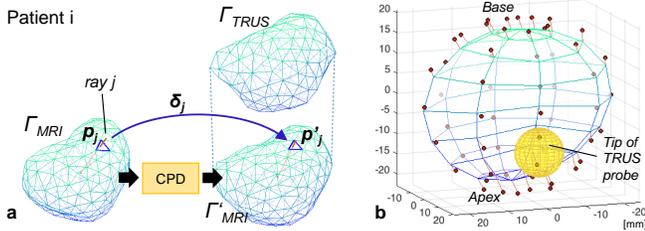
Fig. 1. **a)** Determination of prostate shape and deformation vectors corresponding across patients using ray casting technique. **b)** Mean prostate shape **before** (*red vertices*) and after (*mesh*) SDM mean deformation (*red lines*), showing the compression induced by ultrasound transducer (*yellow sphere*).

methods without the need for manual or semi-automatic contouring would be desired.

In this work, we propose a novel, fully automatic MRI/ TRUS registration scheme by combining a statistical deformation model (SDM) generated from a population of clinically observed prostate deformations with an intensity-based image registration algorithm that does not require a segmentation of unseen datasets. This is different from the work by Tahmasebi et al. [14], where an SDM is employed to estimate eigenmodes using a set of known landmark-based deformations, which are then used to extrapolate a likely whole-gland deformation without considering image intensities. Instead of merely incorporating the SDM as regularizer to penalize unlikely, i.e. physically unrealistic deformations as in [15], we directly optimize for eigenmode coefficients, greatly reducing the dimensionality of the registration problem. To improve the performance of the image fusion at critical lesions, as key element of our method, we propose to anisotropically precondition the image similarity metric, emphasizing the importance of accurate alignment not only at likely cancer locations visible in PSMA-PET images but also predominantly along the main directions of expected deformation.

2. METHOD

Statistical Deformation Model. The generation of the SDM is based on a dataset of N corresponding pre-interventional MR images I_{MR} and interventional TRUS images I_{US} acquired respectively in the supine and lithotomy positions.

Similar to the approach in [5], triangular surface meshes of the prostate are created from available binary segmentations in both images (Γ_{MR}, Γ_{US}), and demeaned so that their center of gravity is at the origin. As shown in Fig. 1a, their vertices are elastically registered with the Coherent Point Drift (CPD) algorithm [16] to obtain a warped MR mesh Γ'_{MR}. Due to the arbitrary vertex numbering in the N meshes, point correspondence across patients is established by intersecting M angularly equidistant rays starting at the origin with meshes Γ_{MR} for all patients. Thus, new vertex
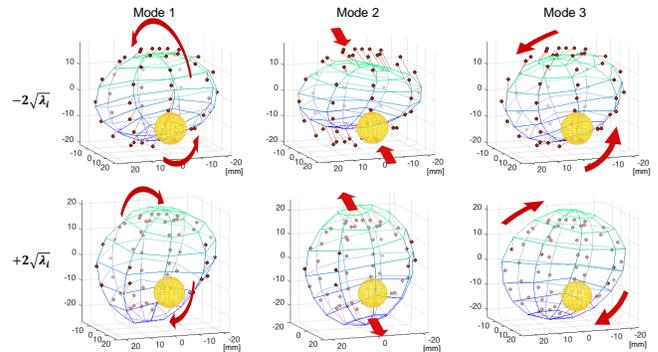
Fig. 2. Deformation caused by the first SDM eigenmodes (*red lines*). Red vertices show the mean prostate **after** average deformation. Red arrows indicate the main direction of deformation (rotation around the left-right axis, compression in the direction of transducer insertion, and rotation around the cranio-caudal axis, respectively).

positions in MR space $\mathbf{p}_{i,j} \in \Gamma_{MR_i}$ and – using barycentric interpolation – in US (i.e. warped MR) space $\mathbf{p}'_{i,j} \in \Gamma'_{MR_i}$ are obtained for patients $i = 1, .., N$ and rays $j = 1, .., M$. The point set $\hat{P}$ of the mean prostate shape in MR, and the mean deformations $\hat{D}$ are then defined as

$$\hat{P} = \{\hat{\mathbf{p}}_j = \frac{1}{N}\sum_{i=1}^{N}\mathbf{p}_{i,j}\}, \qquad \hat{D} = \{\hat{\boldsymbol{\delta}}_j = \frac{1}{N}\sum_{i=1}^{N}\boldsymbol{\delta}_{i,j}\}, \text{ (1)}$$

with $\boldsymbol{\delta}_{i,j} = \mathbf{p}'_{i,j} - \mathbf{p}_{i,j}$ (see Fig. 1a). As in [17], the SDM is created using PCA. In brief, the deformations are demeaned ($\boldsymbol{\delta}'_{i,j} = \boldsymbol{\delta}_{i,j} - \hat{\boldsymbol{\delta}}_j$) and vectorized into matrix $\Delta \in \mathbb{R}^{N \times 3M}$. An Eigen analysis of $\text{cov}(\Delta)$ yields the sorted and devectorized eigenvectors ϕ_k and corresponding eigenvalues λ_k.

Deformable Registration Framework. In general, image registration aims at finding an optimal transformation T^* between reference and moving images, in our case TRUS and MRI, using a similarity metric S and an iterative solver: $T^* = \arg\max_T S[I_{US}, T(I_{MR})]$. Hereby, the similarity metric $S(I_{US}, I'_{MR})$ measures how well fixed image I_{US} and transformed moving image $I'_{MR} = T(I_{MR})$ correspond, commonly by integrating a metric f over the entire overlapping image domain Ω: $S(I_{US}, I'_{MR}) = \int_{\Omega} f(x)\ dx$. In this work, the multi-modal LC^2 similarity metric is employed due to its excellent behavior for MRI/ultrasound registration. In short, LC^2 correlates ultrasound intensities $I_{US}(x)$ with a linear combination of MRI intensities and gradients, see [18] for further details.

Similarity Metric Preconditioning. The aim of the proposed preconditioning is to emphasize the optimization of image alignment at crucial locations $\mathbf{t}$ for a given application. For prostate biopsy guidance, such locations could be suspicious lesions present in MRI and/or PET. In this work, locations $\mathbf{t}$ are automatically identified by the position of maximum PSMA expression in PET images, which are already registered to the corresponding MR images by acquisition (combi-

Table 1. Average registration errors (TRE) in mm for **a)** rigid registration purely based on boundary landmarks (LM), and **b)** surface-based registration as in [5]. **c)** Effect of iso-/anisotropic preconditioning onto TRE for LM placed close to **t** (lesion).

	Experiment	TRE for	1	2	3	4	5	6	7	8	9	10	$\mu \pm \sigma$
a)	Rigid	All LMs	3.63	6.17	1.63	3.18	4.74	2.59	2.41	1.99	3.56	2.14	3.20±1.33
		Lesion	7.13	16.2	1.99	3.91	4.42	1.47	3.16	1.16	4.91	3.44	4.78±4.16
b)	Surface-based [5]	All LMs	3.09	2.34	1.35	8.40	3.01	4.65	4.50	6.26	5.46	4.91	4.40±1.95
		Lesion	0.32	2.03	2.48	7.96	1.60	1.65	4.33	2.64	2.36	5.99	3.14±2.19
c)	Without Preconditioning	All LMs	2.85	2.65	4.26	2.31	4.75	3.40	2.83	1.97	2.60	3.35	3.10±0.82
		Lesion	2.16	3.25	1.20	1.48	1.84	2.37	1.61	0.79	2.13	1.73	**1.86±0.64**
	Isotropic Preconditioning (ζ_{iso})	All LMs	1.88	3.64	2.87	2.39	4.71	3.07	3.03	2.08	6.26	3.48	3.34±1.25
		Lesion	2.28	2.37	1.27	1.31	1.54	2.15	1.20	1.14	1.74	1.87	**1.69±0.44**
	Anisotropic Preconditioning (ζ_{aniso})	All LMs	2.71	3.90	2.96	2.36	5.03	3.91	2.85	2.68	5.42	2.79	3.46±1.01
		Lesions	0.84	2.47	1.31	1.24	1.08	2.39	1.18	0.478	2.06	1.09	**1.41±0.63**

ned scanner). We propose to modify the metric of the otherwise Euclidean space for integration as follows:

$$S(\mathrm{I}_{US}, \mathrm{I}'_{MR}) = \int_{\Omega} f(x) \underbrace{\zeta(x) \, dx}_{\text{metric change}} . \quad (2)$$

The function $\zeta(x) \in [0, 1]$ modifies the "density" of the image space, effectively emphasizing the registration on areas where ζ is close to 1, and removing influence of areas where ζ is close to 0. A simple, isotropic (i.e. direction-independent) preconditioning around **t** can now be achieved using the logistic function and the Euclidean norm:

$$\zeta_{iso}(x) = 1 - \left(1 + e^{-k \cdot (\|x - \mathbf{t}\| - d_0)}\right)^{-1}, \quad (3)$$

where parameters k and d_0 control logistic slope and the curve's inflection point, respectively. Zikic et al. [19] used location-independent gradient normalization to improve mutual information-based registration. The idea of our approach is to not only focus the registration on the region around **t** but also predominantly along the expected directions of deformation at **t**. To this end, we estimate the deformations $\mathbf{d}_k$ at this point using the first three SDM eigenmodes $\sqrt{\lambda_k} \cdot \phi_k$, for $k = 1, 2, 3$, and thin-plate splines (TPS) for interpolation between control points. Note that because the TPS interpolation does not guarantee a linear mapping, the deformations' covariance matrix $\Sigma = \mathrm{cov}([\mathbf{d}_1 \, \mathbf{d}_2 \, \mathbf{d}_3])$ is not necessarily diagonal. Denoting $\|x - \mathbf{t}\|_{\Sigma} = \sqrt{(x - \mathbf{t})^{\intercal} \Sigma^{-1} (x - \mathbf{t})}$ the Mahalanobis distance with respect to location **t**, we propose the anisotropic preconditioning function (example in Fig. 3f):

$$\zeta_{aniso}(x) = 1 - \left(1 + e^{-k \cdot (\|x - \mathbf{t}\|_{\Sigma} - d_0)}\right)^{-1}. \quad (4)$$

Automatic Deformable Registration Workflow. First, both MRI and ultrasound images are rigidly aligned. A reasonably good rotatory initialization is achieved using the acquisition setup (see Sec. 3). In terms of translation, both images are first aligned to the center of the image, followed by a rigid registration using LC^2. For the essential part of the proposed registration scheme, we formulate a deformation field using a linear combination of the SDM eigenmodes. For each control point $\hat{\mathbf{p}}_j$, i.e. vertex of the mean prostate shape, the corresponding deformation is defined as follows: $\mathbf{d}_j = (1 + \theta_0) \cdot \hat{\boldsymbol{\delta}}_j + \sum_{k=1}^{L} \theta_k \cdot \sqrt{\lambda_k} \cdot \phi_k$, where L is the number of used eigenmodes, and $\boldsymbol{\theta} = (\theta_0, ..., \theta_L)$ the vector of optimization parameters. For registration, we now directly optimize for an optimal parametrization $\boldsymbol{\theta}^* = \arg\max_{\boldsymbol{\theta}} S[\mathrm{I}_{US}, T_d(\mathrm{I}_{MR}, \boldsymbol{\theta})]$. Hereby, $T_d(x, \boldsymbol{\theta}) = x + D(x, \boldsymbol{\theta})$ denotes the elastic transformation with the dense deformation field D created using thin-plate splines (TPS) as in [5] for efficient GPU image warping. Note that θ_0 allows to scale the mean deformation, allowing to cope with various probe pressures during US acquisition.

3. RESULTS AND DISCUSSION

Dataset and Experimental Setup. In total, $N = 50$ patient datasets[1] of prostate MRI and TRUS were acquired as in [5], including automatic TRUS segmentation using a Hough forest and manual MR segmentation by an expert, both of which are used for SDM generation. In addition, for a subset of 10 datasets, a corresponding PSMA-PET image for automatic identification of locations **t** for preconditioning, manual TRUS segmentations and six corresponding landmark points in both modalities (four at the prostate boundary, two at structures within the organ, all manually annotated by an expert) were available. For each patient, we asked for one landmark point to be placed in the vicinity of **t**, ideally not farther away than 5 mm. To test the accuracy of the Hough forest, the Dice score between automatic and additionally obtained manual US segmentation in the mid-gland region was found to be 86.2±3.5 for these 10 patients, which is similar to the ones reported in [5, 11] and indicates potentials for improvement.

Statistical Deformation Model. Fig. 1b shows the mean deformation and Fig. 2 the first three eigenmodes of the SDM generated using $M = 81$ rays and the 50 automatic TRUS

---

[1]Informed consent was obtained from all individual participants included in the study, which was performed in accordance with the ethical standards of the institutional and national research committees.
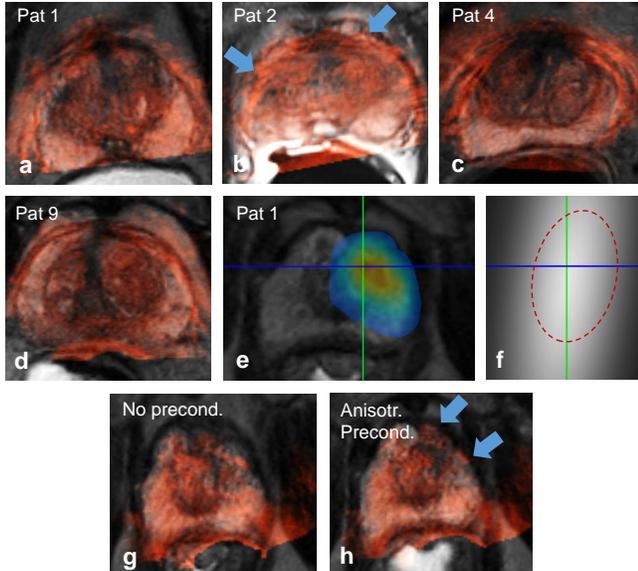
Fig. 3. **a-d**) Registration result for four example datasets shown as axial slice overlays of the TRUS image (*red*) onto warped MR (*greyscale*). For Pat. 2, the registration got stuck in a local minimum (*blue arrows*). **e**) MRI with PET overlay for one patient in the apical region, with selection lesion **t**. **f**) Preconditioning weight map ζ_{aniso}, with estimated main directions of deformation (*ellipse*), allowing to improve registration without preconditioning (**g**) compared to the proposed anisotropic preconditioning (**h**, *blue arrows*).

segmentations only. While all three induce a volume change, compression is most prominent in the second mode (95% variation between $\pm 2\sqrt{\lambda}$). Already the first 9 eigenmodes were found to explain 92% of the variation in the dataset, suggesting that despite the variation in prostate size, the expected deformations during a biopsy session compared to the patient's pose in the MRI scanner are quite homogeneous. We therefore assume that an SDM can capture the patient-specific deformations reasonably well.

Deformable Registration. We validate our approach on the 10 fully annotated datasets, excluding the dataset under investigation from SDM generation, using target registration
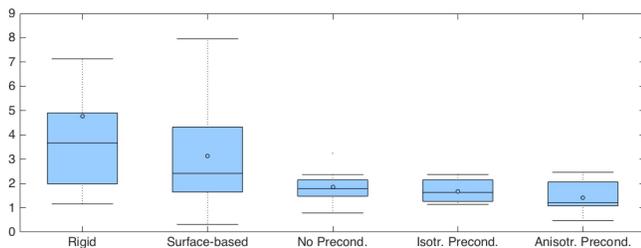
Fig. 4. Target registration errors (TRE) in mm for the landmarks placed close to **t** (lesion), showing that the proposed method outperforms rigid and surface-based registration, and that anisotropic preconditioning can improve alignments around critical structures.

error (TRE) of the landmark points. We optimized for the first $L = 9$ eigenmodes, together with θ_0 leading to a total of 10 parameters. Empirically identified parameters $d_0 = 40$ and $k = 0.001$ were used for preconditioning. All results are reported in Tab. 1. The rigid registration (Tab. 1a) was computed purely based on the four boundary landmarks using the Umeyama method, clearly showing that rigid registrations are inappropriate for this application (errors of up to 16.2 mm). Surface-based registration as in [5] (Tab. 1b) was better than rigid fusion for many cases but showed severe misalignments, mostly due to inaccurate automatic segmentation, in the few cases where it failed. Representative examples of the proposed method (results in Tab. 1c) are depicted in Fig. 3a-d, with e-h showing the effect of the preconditioning. TREs of the lesion-specific landmarks suggest that, as expected, anisotropic preconditioning performs better than the other two options, decreasing the average error from 1.86 and 1.69 mm to 1.41 mm. Results indicate that improvements towards the critical lesion can affect the registration accuracy at other locations, which might be an acceptable trade-off for targeted prostate biopsies. Errors obtained using the proposed method were in the range of the experiments conducted in [11, 20]. After our registration pipeline, the average Hausdorff distance between ground truth MRI and TRUS meshes was 1.84 ± 0.59 mm. The obtained results do not only show that an SDM can be used to elastically register unseen patient MR and TRUS images but also that inaccuracies in the segmentation process, as required for SDM generation using a large dataset, can be overcome by the optimizer. However, the high inter-subject variability might be reduced by SDM generation with an even more extensive training set.

Lesion-specific landmark TREs are also reported in Fig. 4 for all evaluated methods. Paired Kolmogorov-Smirnov tests indicate that all SDM-based methods performed significantly better than rigid registration ($p < 0.05$), and that the proposed SDM registration with anisotropic preconditioning performs significantly better than surface-based registration. Due to various graphics processor optimizations, the runtime for the entire registration pipeline was on average 17.5 seconds, roughly $6\times$ faster than [20] and thus well suited for the tight time requirements of clinical routine.

4. CONCLUSION

In this work, we have presented a statistical deformation model between prostate MRI and TRUS based on automatic US segmentations, and successfully incorporated it into a novel fully automatic, segmentation-free, intensity-based registration framework. Together with the proposed anisotropic similarity preconditioning, we reached promising registration errors, especially around crucial regions of interest for lesion biopsy targeting. Potential future extensions include the generation of more detailed models, strategies to avoid local minima issues and a more extensive (pre-)clinical validation.

5. REFERENCES

[1] M A Bjurlin, J S Wysock, and S S Taneja, "Optimization of prostate biopsy: review of technique and complications," *Urologic Clinics of North America*, vol. 41, no. 2, pp. 299–313, 2014.

[2] T Maurer, M Eiber, M Schwaiger, and J Gschwend, "Current use of PSMA-PET in prostate cancer management," *Nature Reviews Urology*, vol. 13, no. 4, pp. 226–235, 2016.

[3] M M Siddiqui, S Rais-Bahrami, B Turkbey, A K George, J Rothwax, N Shakir, et al., "Comparison of MR/ultrasound fusion–guided biopsy with ultrasound-guided biopsy for the diagnosis of prostate cancer," *Jama*, vol. 313, no. 4, pp. 390–397, 2015.

[4] S Xu, J Kruecker, P Guion, N Glossop, Z Neeman, P Choyke, A K Singh, and B J Wood, "Closed-loop control in fused MR-TRUS image-guided prostate biopsy," in *MICCAI 2007. LNCS*, pp. 128–135. Springer, 2007.

[5] O Zettinig, A Shah, C Hennersperger, M Eiber, C Kroll, H Kübler, et al., "Multimodal image-guided prostate fusion biopsy based on automatic deformable registration," *International journal of computer assisted radiology and surgery*, vol. 10, no. 12, pp. 1997–2007, 2015.

[6] J Mitra, Z Kato, R Martí, A Oliver, X Lladó, D Sidibé, S Ghose, J C Vilanova, J Comet, and F Meriaudeau, "A spline-based non-linear diffeomorphism for multimodal prostate registration," *Med Image Anal*, vol. 16, no. 6, pp. 1259–1279, 2012.

[7] A Sotiras, C Davatzikos, and N Paragios, "Deformable medical image registration: A survey," *Medical Imaging, IEEE Transactions on*, vol. 32, no. 7, pp. 1153–1190, 2013.

[8] B Glocker, N Komodakis, N Navab, G Tziritas, and N Paragios, "Dense registration with deformation priors," in *Information processing in medical imaging*. Springer, 2009, pp. 540–551.

[9] J Wouters, E D'Agostino, F Maes, D Vandermeulen, and P Suetens, "Non-rigid brain image registration using a statistical deformation model," in *Medical imaging*. International Society for Optics and Photonics, 2006, pp. 614411–614411.

[10] J A Onofrey, L H Staib, S Sarkar, R Venkataraman, and X Papademetris, "Learning nonrigid deformations for constrained point-based registration for image-guided MR-TRUS prostate intervention," in *Biomedical Imaging (ISBI), 2015 IEEE 12th International Symposium on*. IEEE, 2015, pp. 1592–1595.

[11] A Fedorov, S Khallaghi, C A Sánchez, A Lasso, S Fels, K Tuncali, et al., "Open-source image registration for MRI–TRUS fusion-guided prostate interventions," *International journal of computer assisted radiology and surgery*, vol. 10, no. 6, pp. 925–934, 2015.

[12] Y Wang, D Ni, J Qin, M Lin, X Xie, M Xu, and P A Heng, "Towards personalized biomechanical model and mind-weighted point matching for robust deformable MR-TRUS registration," in *Computer-Assisted and Robotic Endoscopy*, pp. 121–130. Springer, 2014.

[13] Y Hu, E Gibson, H U Ahmed, C M Moore, M Emberton, and D Barratt, "Population-based prediction of subject-specific prostate deformation for MR-to-ultrasound image registration," *Medical image analysis*, vol. 26, no. 1, pp. 332–344, 2015.

[14] Amir M Tahmasebi, Reza Sharifi, Harsh K Agarwal, Baris Turkbey, Marcelino Bernardo, Peter Choyke, Peter Pinto, Bradford Wood, and Jochen Kruecker, "A statistical model-based technique for accounting for prostate gland deformation in endorectal coil-based mr imaging," in *2012 Annual International Conference of the IEEE Engineering in Medicine and Biology Society*. IEEE, 2012, pp. 5412–5415.

[15] Srivathsan Koundinyan, Robert Toth, Anant Madabhushi, and Timothy Maguire, "A statistical deformation model based regularizer for registration of histology and mri," in *2014 40th Annual Northeast Bioengineering Conference (NEBEC)*. IEEE, 2014, pp. 1–2.

[16] A Myronenko and X Song, "Point set registration: Coherent point drift," *IEEE Trans. Pattern Anal. Mach. Intell.*, vol. 32, no. 12, pp. 2262–2275, 2010.

[17] D Rueckert, A F Frangi, and J A Schnabel, "Automatic construction of 3-d statistical deformation models of the brain using nonrigid registration," *Medical Imaging, IEEE Transactions on*, vol. 22, no. 8, pp. 1014–1025, 2003.

[18] B Fuerst, W Wein, M Müller, and N Navab, "Automatic ultrasound–MRI registration for neurosurgery using the 2D and 3D LC2 metric," *Med Image Anal*, vol. 18, no. 8, pp. 1312–1319, 2014.

[19] D Zikic, M Baust, A Kamen, and N Navab, "A general preconditioning scheme for difference measures in deformable registration," in *Computer Vision (ICCV), 2011 IEEE International Conference on*. IEEE, 2011, pp. 49–56.

[20] Y Sun, J Yuan, M Rajchl, W Qiu, C Romagnoli, and A Fenster, "Efficient convex optimization approach to 3D non-rigid MR-TRUS registration," in *Medical Image Computing and Computer-Assisted Intervention– MICCAI 2013*, pp. 195–202. Springer, 2013.